Soft Matter

PAPER

View Article Online
View Journal | View Issue

Published on 02 August 2016. Downloaded by University of South Carolina Libraries on 14/12/2016 21:25:24.

Cite this: *Soft Matter*, 2016, 12, 7241

Role of block copolymer adsorption *versus* bimodal grafting on nanoparticle self-assembly in polymer nanocomposites†

Dan Zhao,[a] Matteo Di Nicola,[b] Mohammad M. Khani,[c] Jacques Jestin,[ad] Brian C. Benicewicz[c] and Sanat K. Kumar*[a]

Received 17th June 2016,
Accepted 1st August 2016

DOI: 10.1039/c6sm01396a

www.rsc.org/softmatter

We compare the self-assembly of silica nanoparticles (NPs) with physically adsorbed polystyrene-*block*-poly(2-vinylpyridine) (PS-*b*-P2VP) copolymers (BCP) against NPs with grafted bimodal (BM) brushes comprised of long, sparsely grafted PS chains and a short dense carpet of P2VP chains. As with grafted NPs, the dispersion state of the BCP NPs can be facilely tuned in PS matrices by varying the PS coverage on the NP surface or by changes in the ratio of the PS graft to matrix chain lengths. Surprisingly, the BCP NPs are remarkably better dispersed than the NPs tethered with bimodal brushes at comparable PS grafting densities. We postulate that this difference arises because of two factors inherent in the synthesis of the NPs: In the case of the BCP NPs the adsorption process is analogous to the chains being "grafted to" the NP surface, while the BM case corresponds to "grafting from" the surface. We have shown that the "grafted from" protocol yields patchy NPs even if the graft points are uniformly placed on each particle. This phenomenon, which is caused by chain conformation fluctuations, is exacerbated by the distribution function associated with the (small) number of grafts per particle. In contrast, in the case of BCP adsorption, each NP is more uniformly coated by a P2VP monolayer driven by the strongly favorable P2VP–silica interactions. Since each P2VP block is connected to a PS chain we conjecture that these adsorbed systems are closer to the limit of spatially uniform sparse brush coverage than the chemically grafted case. We finally show that the better NP dispersion resulting from BCP adsorption leads to larger mechanical reinforcement than those achieved with BM particles. These results emphasize that physical adsorption of BCPs is a simple, effective and practically promising strategy to direct NP dispersion in a chemically unfavorable polymer matrix.

Introduction

There has been continuing interest in dispersing inorganic nanoparticles (NPs) into an organic polymer matrix with the ultimate goal of synthesizing materials with improved properties.[1–6] However, in most cases, the inorganic NPs and the organic polymer phase are energetically immiscible, with the resulting particle agglomeration leading to only minor property enhancements. To overcome this difficulty, many strategies have been proposed in the past few decades for manipulating the enthalpic and entropic interactions between these two components so as to facilitate their miscibility.[7–10] One promising way is to chemically graft the particle surface with polymer chains and mixing them with matrices possessing the same chemistry as the brush.[11] In such cases, miscibility at high grafting density is driven by the entropy of mixing between the brush and the matrix chains.[9,12,13] More interestingly, at low grafting densities (*e.g.*, $\sigma < 0.1$ chains per nm^2), the NPs self-assemble into anisotropic superstructures through a compromise between this mixing entropy and the attraction between the NP cores.[8,14,15] Recently, bimodal (BM) brushes have been used, in which a sparsely grafted, long brush provides a miscible interface with the bulk polymer while a densely grafted, short brush helps reduce the inter-particle van der Waals attraction, to further improve the dispersion of NPs.[16–19]

While this chemical grafting idea has resulted in much success in lab-scale practice, it typically involves complicated

[a] *Department of Chemical Engineering, Columbia University, 500 West 120th Street, New York, New York 10027, USA. E-mail: sk2794@columbia.edu*
[b] *School of Science and Technology, Università di Camerino, Via Sant'Agostino 1, 62032, Camerino, Italy*
[c] *Department of Chemistry and Biochemistry, University of South Carolina, Columbia, South Carolina 29208, USA*
[d] *Laboratoire Léon Brillouin, CEA Saclay, 91191 Gif-sur-Yvette Cedex, France*

† Electronic supplementary information (ESI) available: DLS measurements for adsorption of 110-*b*-12.5 BCP onto silica; additional TEM micrographs; van der Waals attraction potential *vs.* interparticle separation; $C(r)$ analysis; loss modulus data, strain sweep results for linear rheology. See DOI: 10.1039/c6sm01396a

Published on 02 August 2016. Downloaded by University of South Carolina Libraries on 14/12/2016 21:25:24.

chemistry making it too time-intensive and costly to be realized on an industrial scale. To resolve this difficulty, we recently proposed a simpler strategy to disperse silica NPs into a chemically unfavorable polystyrene (PS) matrix. We modified the NP surface with a physically adsorbed monolayer of polystyrene-*block*-poly(2-vinylpyridine) (PS-*b*-P2VP) copolymers (BCP).[20] In this case, the short P2VP block, which adsorbs to the NP surface due to the favorable interactions with the silanol groups,[21,22] also helps to reduce inter-core attractions.[23] In addition, the long PS block provides a miscible interface with the matrix chains. As a consequence, we have found that the BCP NPs are uniformly dispersed in the PS matrices even at a grafting density of 0.01 chains per nm^2- similar results can only be attained at an order of magnitude higher grafting density for monomodal grafted NPs. These results strongly suggest that the idea of reducing inter-NP attraction, and allowing for the favorable mixing of the brush and the matrix chains can be achieved with BCP NPs. Here, we contrast two methods of reducing inter-NP attractions: in addition to BCP approach discussed above, we will use bimodal brush grafted NPs, with a short dense P2VP brush used to reduce inter-NP attractions and a long PS brush to improve the miscibility with the matrix. We then compare the dispersion behavior as well as its consequence on the viscoelastic properties in the two cases. With these results, we aim to address the following questions: (i) Is physically adsorbing polymer molecules equivalent in terms of NP dispersion to chemically grafting the chains onto the NPs? If not, in what tangible ways are they different and what is the underlying physics leading to the observed difference? (ii) How does the presence of the short P2VP block/brush affect these results? (iii) What are the implications on the mechanical reinforcement in these two different classes of hybrids?

Materials and methods

Materials

All materials were used as received. Methylethylketone (MEK, HPLC-grade, >99.7%) and tetrahydrofuran (THF, ACS agent, >99.0%) was purchased from Sigma-Aldrich. PS with varying molecular weights (M_w = 42 kg mol^{-1}, $Đ$ (dispersity) = 1.05; M_w = 106 kg mol^{-1}, $Đ$ = 1.06; M_w = 119.6 kg mol^{-1}, $Đ$ = 1.04; M_w = 592 kg mol^{-1}, $Đ$ = 1.09; M_w = 1050 kg mol^{-1}, $Đ$ = 1.08) and PS-*b*-P2VP BCPs (M_n = 148.5-*b*-19 kg mol^{-1}, $Đ$ = 1.05, denoted as 148.5-*b*-19 in the text; M_n = 110-*b*-12.5 kg mol^{-1}, $Đ$ = 1.09, denoted as 110-*b*-12.5) were obtained from Polymer Source. The colloidal silica NPs (MEK-ST, 10–15 nm in diameter) and the antioxidant Irganox 1010 used in this work were donated by Nissan Chemical Industries and Ciba Specialty Chemicals (now BASF Switzerland), respectively.

Nanocomposite preparation and processing

The solvent casting method is used to prepare the nanocomposites studied in this work. First, solutions of 0.1 wt% silica in MEK were prepared by diluting the as-received stock particle suspension (~31 wt% in silica). Second, measured amounts of PS-*b*-P2VP were added to the silica solution. The resulting silica/PS-*b*-P2VP dispersions were vortex mixed for 24 h to ensure complete BCP dissolution and adsorption. Following that, homopolymer PS of a desired molecular weight and antioxidant (0.5 wt% relative to the polymer) were blended with the silica/PS-*b*-P2VP solutions. The resulting mixtures were left on a vortex mixer for another 24 h, poured into a PTFE petri dish and air-dried in a fume hood for several days. We have also synthesized bimodal PS–P2VP grafted silica NPs (the silica core is Nissan MEK-ST) using the reversible addition–fragmentation chain transfer (RAFT) polymerization[16] and incorporated them into PS matrices following similar procedures as described above. The grafting characteristics of the bimodal PS–P2VP coated silica NPs are as follows: (i) M_n = 7.5 kg mol^{-1}, $Đ$ (dispersity) = 1.15, and σ_{P2VP} (grafting density) = 0.18 chains per nm^2 for the P2VP brush; M_n = 104 kg mol^{-1}, $Đ$ = 1.4 and σ_{PS} = 0.02 chains per nm^2 for the PS brush, denoted as BM-0.02-104 and (ii) M_n = 6 kg mol^{-1}, $Đ$ (dispersity) = 1.09, and σ_{P2VP} (grafting density) = 0.18 chains per nm^2 for the P2VP brush; M_n = 157 kg mol^{-1}, $Đ$ = 1.4 and σ_{PS} = 0.05 chains per nm^2 for the PS brush, denoted as BM-0.05-157. To completely remove all residual solvent and equilibrate the NP structures in the matrices, the as-cast samples are thermally annealed for 5 days at 150 °C under vacuum. The final dry nanocomposites contain 5 wt% silica core.

Quasi-elastic light scattering (DLS)

The light scattering experiments were conducted on a BI-200SM (Brookhaven Instruments) instrument equipped with a diode-pumped solid state (DPSS) laser operating at λ = 532 nm and a BI-9000 AT digital correlator. In a typical test, a solution containing 0.1 wt% silica NP (or ~0.037 vol%) and a varying content of PS-*b*-P2VP was prepared and filtered with a 0.45 μm PTFE filter prior to each measurement. For comparison, all the measurements were conducted at a fixed scattering angle, *i.e.*, 90°. The apparent hydrodynamic diameter (D_H) of the test particles were then estimated from the measured effective diffusion coefficient according to the Stokes–Einstein relation.

Transmission Electron Microscopy (TEM)

To characterize the spatial organization of particles in real space, the bulk nanocomposite film was ultramicrotomed into slices with thickness ~60 nm using a diamond knife. A string of these sections was then floated on a Formvar-coated copper TEM grid from deionized water and visualized in a JEOL JEM-100 CX or Philips CM-12 electron microscope operating at an accelerating voltage of 100 kV.

Rheology

A strain-controlled ARES-G2 rheometer (TA Instruments) equipped with 8 mm parallel plates was used for rheological characterization. The annealed samples were compression molded into 8 mm discs using a custom molding apparatus. The rheology measurements were performed at different temperatures (160–200 °C, well above the glass transition temperature T_g ~ 100 °C of neat PS) under nitrogen and a master curve

 This journal is © The Royal Society of Chemistry 2016

Published on 02 August 2016. Downloaded by University of South Carolina Libraries on 14/12/2016 21:25:24.

for each sample was created following the time–temperature superposition principle. Prior to the frequency-sweep test, we first run a strain-sweep experiment at the maximum frequency to determine the range of linear strains (Fig. S7 and S8, ESI†).

Results and discussion

The system consists of PS matrices of varying molecular weights and silica NPs with either physically adsorbed PS-*b*-P2VP BCPs or chemically grafted PS–P2VP brushes. The NP grafting characteristics and the nomenclature used are presented in Table 1. To facilitate the discussion below, the BCPs are denoted as M_n(PS)-*b*-M_n(P2VP), where M_n(PS) and M_n(P2VP) are the number-averaged molecular weight of the PS and P2VP block in kg mol^{-1}, respectively. The BCP coated NPs are denoted as BCP-σ-M_n(PS), where σ is the adsorbing or "grafting" density of the BCPs. For example, the NPs fully adsorbed with 148.5-*b*-19 BCPs will be denoted as BCP-0.01-148.5.

Adsorption of BCPs onto silica NPs

Fig. 1 presents the hydrodynamic diameter (D_H) obtained from DLS on silica/PS-*b*-P2VP (148.5-*b*-19) dispersions in MEK as a function of PS-*b*-P2VP solution concentration ($C_{PS\text{-}b\text{-}P2VP}$). For these measurements, the silica concentration is kept fixed at 0.1 wt%. In the case of pure silica NPs, we found an average D_H of ~22.4 nm (Fig. 1). Note that the larger size obtained, relative to the geometric size of MEK-ST (~14 ± 4 nm in diameter), is due to polydispersity, and also because the hydrodynamic size is known to be larger than the geometric size. With the addition of PS-*b*-P2VP, D_H increases abruptly but then remains essentially unchanged upon further increases of $C_{PS\text{-}b\text{-}P2VP}$ up to 0.4 g L^{-1}. According to our previous studies,[20,22] the attraction strength between silica, P2VP and MEK follows the order: silica/P2VP > silica/MEK > silica/PS. As a consequence, the silica NPs adsorb a monolayer of PS-*b*-P2VP with the P2VP as the sticky, adsorbed block and the PS buoy block excluded from the particle surface. This adsorption process should be self-limiting due to the limited number of NP surface adsorption sites, giving rise to the plateau in D_H at high $C_{PS\text{-}b\text{-}P2VP}$. Going further, the maximum adsorption or grafting density of PS-*b*-P2VP on silica is estimated to be ~0.01 chains per nm^2 (corresponding roughly to ~6 chains per particle) based on the cross-over concentration (~0.4 g L^{-1}) where D_H starts to level off, with the assumption that all the BCPs in solution adsorb onto the particle surface.[21] These results clearly reveal that PS-*b*-P2VP strongly binds to the silica surface even at low concentrations (This has also been confirmed by using another BCP, *i.e.*, 110-*b*-12.5, see Fig. S1, ESI†). Further, the surface coverage of the BCP on the silica NPs can be manipulated by changing the amount of BCPs in solution under the assumption that all the BCPs adsorb under these sub-saturated conditions. Our goal here is to control the assembly of these BCP NPs in PS matrices, as discussed below.

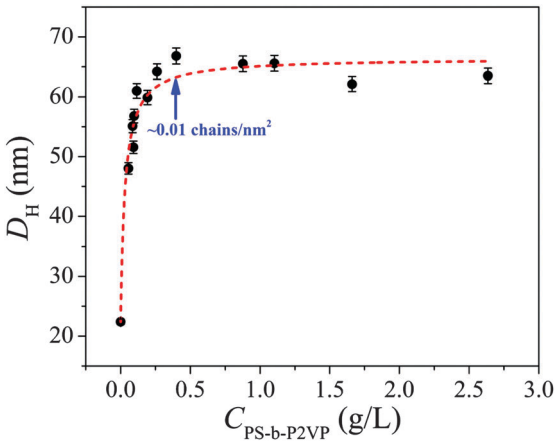

Fig. 1 The apparent hydrodynamic diameter (D_H) of silica/PS-*b*-P2VP (148.5-*b*-19) dispersions in MEK as a function of PS-*b*-P2VP concentration ($C_{PS\text{-}b\text{-}P2VP}$). The weight fraction of silica is kept fixed at 0.1%. The dashed red line is a guide for the eye. The blue arrow indicates the approximate critical concentration, corresponding to σ = 0.01 chains per nm^2.

Dispersion behavior of BCP NPs

We first examine the effect of BCP adsorption on the dispersion of silica NPs in PS matrices. Fig. 2 presents the dispersion behavior of silica NPs with varying amounts of PS-*b*-P2VP (148.5-*b*-19) blended with a 119.6 kg mol^{-1} PS matrix. In the absence of BCPs, the NPs form micron-sized spherical phase separated agglomerates, presumably due to the strongly unfavorable enthapic interactions between the silica and the PS (Fig. 2a, also see Fig. S2a and b, ESI†). Interestingly, with a gradual increase of BCP coverage, the NP morphology can be tuned from large spherical agglomerates (Fig. 2a), small aggregates (Fig. 2b), connected/branched structures (Fig. 2c) to mixtures of short strings and individual particles (Fig. 2d). Specifically, the NPs

Table 1 The grafting characteristics and nomenclature of silica NPs coated by either physically adsorbed BCPs or chemically functionalized bimodal brushes

	P2VP block/brush			PS block/brush			
Type	M_n (kg mol^{-1})	$Đ$	σ_{P2VP} (chains per nm^2)	M_n (kg mol^{-1})	$Đ$	σ_{PS} (chains per nm^2)	Nomenclature
Bimodal	6	1.09	0.18	157	1.4	0.05	BM-0.05-157[a]
Bimodal	7.5	1.15	0.18	104	1.4	0.02	BM-0.02-104[a]
BCP	19	1.05	0.01	148.5	1.05	0.01	BCP-0.01-148.5[b]
BCP	12.5	1.09	0.01	110	1.09	0.01	BCP-0.01-110[b]

[a] These two particles are chemically grafted with bimodal brushes; they are named following the grafting density and chain length of the PS brush. [b] Particles with physically adsorbed BCPs; the nomenclature is based on the characteristics of the PS block. In this table we have only shown the particles fully adsorbed by BCPs. For those with less BCPs, the grafting density can range from 0–0.01 chains per nm^2.

Published on 02 August 2016. Downloaded by University of South Carolina Libraries on 14/12/2016 21:25:24.

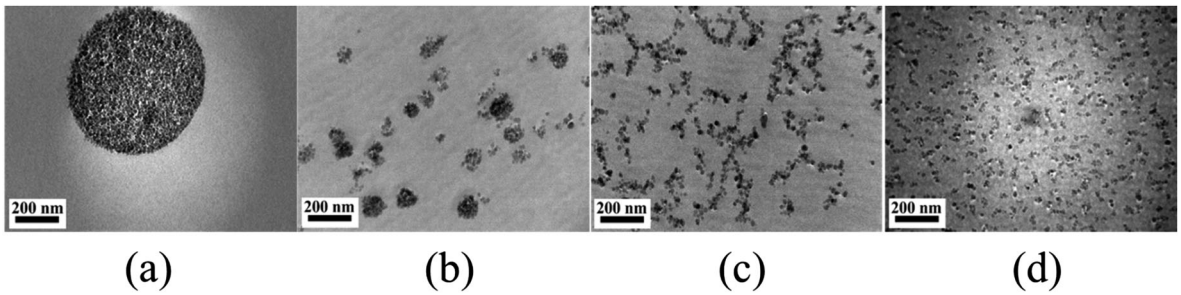

Fig. 2 TEM micrographs for 119.6 kg mol^{-1} PS melts filled with silica NPs adsorbed with different amounts of 148.5-*b*-19 BCPs: (a) $C_{PS\text{-}b\text{-}P2VP}$ = 0 g L^{-1}, or σ = 0 chains per nm^2; (b) $C_{PS\text{-}b\text{-}P2VP}$ = 0.045 g L^{-1}, or σ = 0.001 chains per nm^2; (c) $C_{PS\text{-}b\text{-}P2VP}$ = 0.098 g L^{-1}, or σ = 0.002 chains per nm^2; (d) $C_{PS\text{-}b\text{-}P2VP}$ = 1.5 g L^{-1}, or σ = 0.01 chains per nm^2.

still aggregate at σ = 0.001 chains per nm^2 since the average number of BCPs per particle is less than one, and hence most of the silica surface is uncovered. However, there is a reduction in cluster size, which can be attributed to two facts. First, it is entropically unfavorable to confine the adsorbed chains within large clusters. Second, the adsorbed BCP chains, even in small amounts, provide a more miscible interface between the particle and polymer phase, thus helping stabilize smaller clusters against further agglomeration. Going further, at σ = 0.002 chains per nm^2, where there are ~1.4 chains per NP, we have behavior akin to patchy NPs. Thus, the NPs form anisotropic structures, as experimentally observed by Akcora *et al.*[8] and predicted by the geometric model of Asai *et al.*[14] Finally, when the silica NPs are fully adsorbed by BCPs, they are much better dispersed in the PS matrix, forming short strings and even individual particles (also see Fig. S2c and d, where the 110-*b*-12.5 BCPs were used, ESI†).

This improvement in particle dispersion has been attributed to two important facts: the wettable long PS chains provide interfacial miscibility with the matrix PS chains while the inner P2VP block, which collapses to form a dense layer on the silica surface, reduces the attraction strength between the silica cores.[20] To illustrate this point we note that the adsorption of a 19 kg mol^{-1} P2VP bound layer with a thickness of ~0.28 nm (corresponding to ~6 chains of 148.5-*b*-19 BCPs on one particle) helps significantly decrease the inter-core attraction from ~5 k_BT (for bare NPs) to ~1 k_BT at an interparticle separation of 0.1 nm (Fig. S3, ESI;† note that we assume the P2VP chains are densely packed around the silica particle, as they energetically dislike the matrix PS chains in the melt). To illustrate the importance of this P2VP layer on particle dispersion, we compare the structures formed in the present work with those observed by Akcora *et al.*[8] in the case of monomodal PS grafted silica (PS-*g*-silica) NPs. For instance, we see mixtures of short strings and individual particles when embedding BCP NPs (148.5-*b*-19, 0.01 chains per nm^2, N/P = 1.30, where N and P are the degrees of polymerization for the adsorbed and matrix PS chains, respectively) into the 119.6 kg mol^{-1} PS matrices. In contrast, under similar grafting characteristics, the monomodal PS-*g*-silica NPs form connected/sheet structures. Similarly, in a matrix of 592 kg mol^{-1} PS, the BCPs modified silica particles (N/P = 0.26) display self-assembly into strings (Fig. 3a3), while spherical aggregates are found for those coated with monomodal PS brushes. These results again suggest that, as we have found previously,[24,25] the reduction in the attraction strength between two NP cores shifts the system towards better-dispersed phases.

Going further, we also note that the silica NPs with their surfaces fully adsorbed with BCP are not individually dispersed even in the lowest molecular weight matrices (Fig. 2d, 3a1 and a2). We conjecture that, even at maximum BCP adsorption, some of the P2VP is left exposed to the melt – in our previous work,[20] we have found that silica NPs with adsorbed P2VP homopolymer chains alone form large clusters when placed in a PS matrix. Presumably, the presence of the tethered PS chains reduces this contact between the P2VP and the matrix PS chains, but does not completely alleviate this issue. We have also examined the effect of matrix chain length on NP dispersion. As shown in the first row of Fig. 3, as the molecular weight of the PS matrix increases, the NPs are generally more aggregated. This structural evolution as a function of matrix chain length has also been quantified by correlation function, $C(r)$, calculations for the TEM images, as shown in Fig. S4 (ESI†). In such cases, as $\sigma\sqrt{N} > (N/P)^2$, the autophobic interaction between the matrix and the brush starts to play a role. Apparently, in these high molecular weight matrices loosely-packed NP clusters form – however, inside the clusters we still see the ''string'' motifs.

Bimodal grafting *vs.* BCP adsorption

Next, we compare the dispersion and assembly of BCP NPs *vs.* BM NPs with similar grafting characteristics in the same PS matrices. As shown in Fig. 3 (first row *vs.* third row) and Fig. 4, the BCP NPs (BCP-0.01-148.5) are remarkably better dispersed than those grafted with bimodal brushes (BM-0.02-104) over a broad range of matrix molecular weights (42 kg mol^{-1} to 1050 kg mol^{-1}). To ensure that the observed morphological difference in these two systems is not due to the slight difference in the molecular weight of the tethered PS chains (148.5 kg mol^{-1} *vs.* 104 kg mol^{-1}), we have also examined the dispersion of silica NPs coated by a BCP with a similar chain length for the PS block (110 kg mol^{-1}) and found essentially the same results (Fig. S2c–f, ESI†).

Two facts are noted here. First, the thickness of the P2VP layer around each particle in the bimodal case is much larger

 This journal is © The Royal Society of Chemistry 2016

Published on 02 August 2016. Downloaded by University of South Carolina Libraries on 14/12/2016 21:25:24.

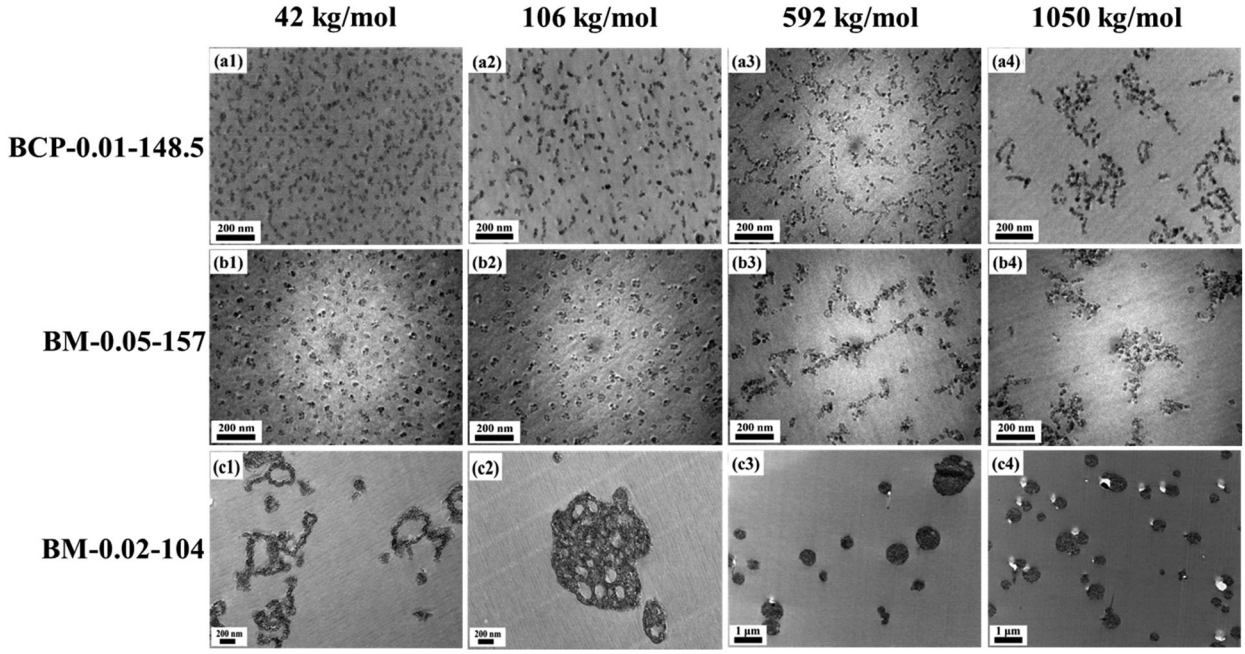

Fig. 3 TEM micrographs for BCP adsorbed (the first row) or bimodal grafted (second and third rows) silica NPs in PS melts with varying molecular weights, as indicated inside the figure.

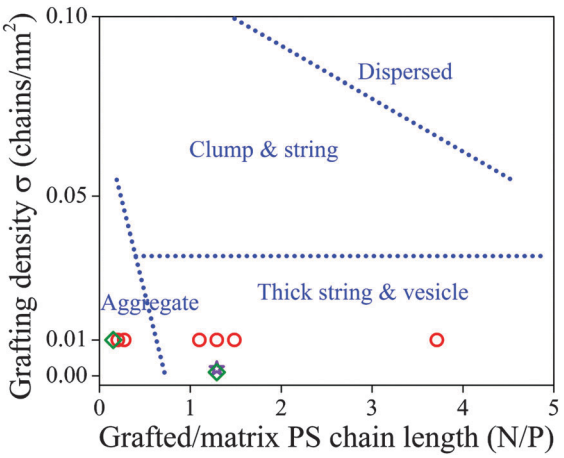

Fig. 4 Comparison of the dispersion state of BCP NPs with that of BM NPs in PS matrices. The diagram shown here is constructed from Ref. 24. The blue dotted lines summarize results from the BM NPs. The symbols shown here correspond to the BCP coated silica NPs, which assemble into different NP morphologies, including "Clump & string" (red circles), "Connected structure" (purple stars) and "Aggregate" (green diamonds).

than that where BCP is used ($\sim$1.63 nm for BM-0.02-104 *vs.* $\sim$0.28 nm for BCP-0.01-148.5, assuming the P2VP chains are completely collapsed onto the silica surface). As a consequence, we expect a smaller attraction between silica cores in the bimodal system (Fig. S3, ESI†). Second, the PS grafting density of the bimodal particles is about twice that of the BCP tethered ones. Both of these results would imply that the BM NPs should be better dispersed than the BCP ones. This is opposite to what we find experimentally. To reconcile these facts we conjecture that the bimodal brush grafted particles expose more of the P2VP to the PS matrix than the BCP NPs, even though on average they have higher grafting densities of the PS brush. We note that the BM brushes are grown from, presumably, randomly chosen surface sites (Fig. 5a, bottom). Inspired by past theories, simulations and experiment[14,26–29] we postulate that, at low grafting density and long grafts, the coverage of PS chains grown in this fashion on the NP surface is anisotropic and asymmetric. Moreover, as discussed by Hakem *et al.*,[30] polydispersity effects in the number of grafted chains per particle add to this anisotropy. In contrast, in the case of BCPs, the chains are "grafted" to the surface by the adsorption of the P2VP segments. Since the BCP adsorption proceeds till the P2VP completely occupies the surface sites, it is clear that the silica NPs should be fully coated by the P2VP block of the BCP chains at a density of 0.01 chains per nm^2. As suggested in Fig. 5a (top) this should lead to a more uniform PS surface coverage of the NPs.

These ideas are consistent with the fact that the BCP modified NPs are significantly better dispersed in the PS matrices as compared to the ones sparsely grafted with mixed bimodal brushes under comparable grafting parameters. To further bolster this idea, we have shown that, to obtain similar NP dispersion states for the adsorbed and grafted systems requires us to increase the grafting density of the BM PS brush to a density of $\sim$0.05 chains per nm^2 (the second row of Fig. 3).

With the dramatic difference in the dispersion states between these two systems under comparable grafting parameters, it would be interesting to examine the impact of this morphological difference on the mechanical properties of the resulting polymer nanocomposites (PNCs). To this end, we have

Published on 02 August 2016. Downloaded by University of South Carolina Libraries on 14/12/2016 21:25:24.

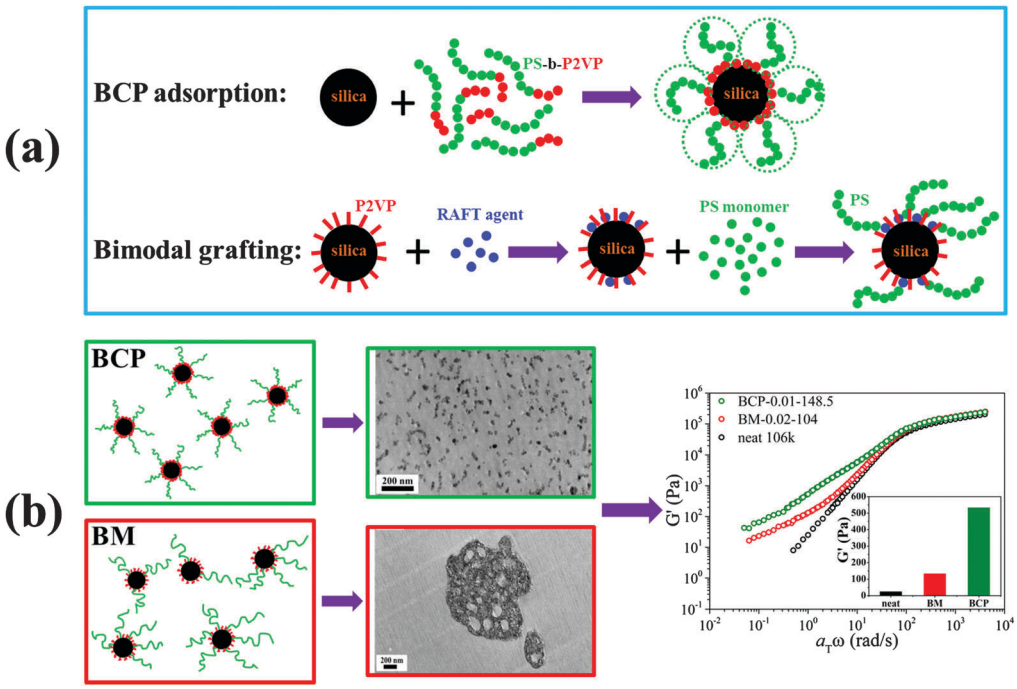

Fig. 5 (a) Illustrating the difference in the process of particle synthesis. In the BCP case, each chain occupies a volume defined by the PS radius of gyration (the dashed circles). Thus the BCPs adsorbing subsequently have to attach to other parts of the surface, ensuring a more uniform surface coverage. While similar physics should apply to the case of bimodal grafting, the excluded volume of the monomeric RAFT agent is much smaller. Thus the distribution of the chains on the NP surface, as well as the number of chains per particle could be strongly non-uniform. (b) Comparison of NP dispersion (TEM micrographs in the middle) and linear viscoelastic properties of 106 kg mol^{-1} PS melts filled with 5 wt% (silica core) BCP-0.01-148.5 (top row) and BM-0.02-104 (bottom row) silica NPs. The cartoons on the left aim to illustrate the structural difference between these two surface-coated NPs on a single-particle level: the BCP ones are more uniformly coated by PS chains while there is fluctuation in both the number of grafted chains per particle and the distribution of grafted chains on the particle surface in the bimodal analogs. Note that, in the cartoons, the black spheres are silica cores; the red and green lines correspond to the P2VP and PS chains, respectively. The plot on the right presents master curves of the storage modulus (G') *vs.* angular frequency ($a_T\omega$) for 106 kg mol^{-1} PS melts (black) as well as those loaded with bimodal brush (red) or BCP (green) tethered silica NPs. The reference temperature is 200 °C, with the shift factors (a_T) shown in Fig. S5 (ESI†). The inset plots the G' at a frequency of 1 rad s^{-1} for the three samples, as indicated inside the graph.

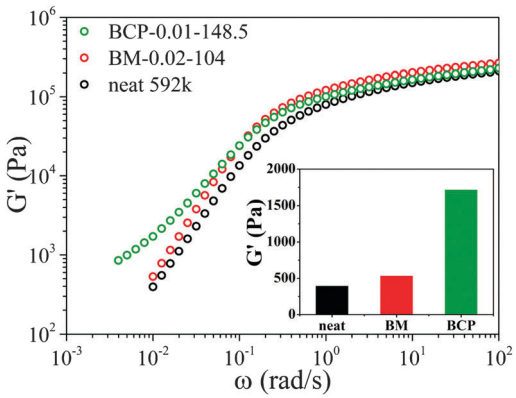

Fig. 6 The storage modulus (G') as a function of angular frequency (ω) for 592 kg mol^{-1} PS melts (black) as well as those loaded with 5 wt% bimodal brush (red) or BCP (green) coated silica NPs. All datapoints shown here were collected at 200 °C. The inset plots the G' at a frequency of 0.01 rad s^{-1} for the three samples, as indicated inside the graph. The data of loss modulus (G'') is not shown here for clarity, which can be found in Fig. S6b (ESI†).

conducted linear viscoelastic measurements on neat PS melts as well as those filled with the NPs of BM-0.02-104 and BCP-0.01-148.5 (Fig. 5b and Fig. 6). First, as expected, with added NPs, the storage modulus (G') of the two PNCs are higher than that for the neat PS melts at all frequencies considered. This reinforcement becomes most pronounced at the smallest rates of deformation.[31,32] For instance, in a 106 kg mol^{-1} matrix (ω = 1 rad s^{-1}), the G' for neat PS is 25 Pa while it is 133 Pa and 534 Pa for PNCs filled with BM and BCP tethered NPs, respectively (inset of Fig. 5b); similarly, in a 592 kg mol^{-1} matrix (ω = 0.01 rad s^{-1}), the G' is 394 Pa, 532 Pa and 1714 Pa for these three samples (inset of Fig. 6). More interestingly, we note that the PNCs loaded with BCP NPs are much more reinforced than those filled with bimodal brush coated ones (*e.g.*, ~4 times larger at ω = 1 rad s^{-1} in 106 kg mol^{-1} PS melts). This low-frequency reinforcement occurs even below the NP percolation threshold (as evidenced by the fact that $G'' > G'$ at low frequencies, see Fig. S6, ESI†) probably reflecting either the slowing down of matrix chain relaxation as a result of the interaction between the grafts and the matrices or due to confinement effects.[32,33] As the BCP tethered NPs are more homogeneously dispersed in the matrices, they should magnify both these effects, thus leading to larger reinforcement as compared to the bimodal case. Our results again suggest that

 This journal is © The Royal Society of Chemistry 2016

Published on 02 August 2016. Downloaded by University of South Carolina Libraries on 14/12/2016 21:25:24.

the dispersion states of NPs in the host polymers are critical to the macroscopic properties of the resulting PNCs, a fact that is well appreciated in the community.[5]

Conclusions

We have systematically examined the dispersion and assembly of silica NPs with physically adsorbed BCPs and those chemically grafted with mixed bimodal brushes in the same PS matrices. First, we show that physical adsorption of BCPs onto silica NPs is a facile means to control NP dispersion and thus the resulting properties. At comparable adsorbing/grafting characteristics, the BCP coated silica NPs are significantly better dispersed than BM NPs in the same matrices. This likely reflects the non-uniform distribution of grafted chains and the distribution of the number of PS chains per particle in the latter case. Finally, we show that PS melts filled with BCP NPs are more reinforced than those consisting of bimodal brush tethered ones, especially at lower frequencies. This can be reconciled by the better dispersion of the BCP NPs relative to their bimodal analogs.

Acknowledgements

The authors are grateful to the National Science Foundation (DMR-1408323) for financial support of this work. We thank Puspanjali Sahu for DLS measurements on silica suspensions adsorbed by 148.5-*b*-19 BCPs. We also would like to thank Erkan Senses and Prof. Pinar Akcora for help with the rheological experiments. NYULMC OCS Microscopy Core is also acknowledged for help with microtome and TEM.

References

1 J. W. Gilman, *Appl. Clay Sci.*, 1999, **15**, 31–49.
2 K. I. Winey, T. Kashiwagi and M. Mu, *MRS Bull.*, 2007, **32**, 348–353.
3 P. Cassagnau, *Polymer*, 2008, **49**, 2183–2196.
4 G. Choudalakis and A. D. Gotsis, *Eur. Polym. J.*, 2009, **45**, 967–984.
5 S. K. Kumar, N. Jouault, B. Benicewicz and T. Neely, *Macromolecules*, 2013, **46**, 3199–3214.
6 D. Zhao, S. Ge, E. Senses, P. Akcora, J. Jestin and S. K. Kumar, *Macromolecules*, 2015, **48**, 5433–5438.
7 M. E. Mackay, A. Tuteja, P. M. Duxbury, C. J. Hawker, B. Van Horn, Z. Guan, G. Chen and R. S. Krishnan, *Science*, 2006, **311**, 1740–1743.
8 P. Akcora, H. Liu, S. K. Kumar, J. Moll, Y. Li, B. C. Benicewicz, L. S. Schadler, D. Acehan, A. Z. Panagiotopoulos and V. Pryamitsyn, *et al.*, *Nat. Mater.*, 2009, **8**, 354–359.
9 C. Chevigny, F. Dalmas, E. Di Cola, D. Gigmes, D. Bertin, F. Boué and J. Jestin, *Macromolecules*, 2010, **44**, 122–133.
10 A. C. Balazs, T. Emrick and T. P. Russell, *Science*, 2006, **314**, 1107–1110.
11 C. Li and B. C. Benicewicz, *Macromolecules*, 2005, **38**, 5929–5936.
12 D. Sunday, J. Ilavsky and D. L. Green, *Macromolecules*, 2012, **45**, 4007–4011.
13 A. P. Gast and L. Leibler, *Macromolecules*, 1986, **19**, 686–691.
14 M. Asai, A. Cacciuto and S. K. Kumar, *Soft Matter*, 2015, **11**, 793–797.
15 P. F. Green, *Soft Matter*, 2011, **7**, 7914–7926.
16 A. Rungta, B. Natarajan, T. Neely, D. Dukes, L. S. Schadler and B. C. Benicewicz, *Macromolecules*, 2012, **45**, 9303–9311.
17 B. Natarajan, T. Neely, A. Rungta, B. C. Benicewicz and L. S. Schadler, *Macromolecules*, 2013, **46**, 4909–4918.
18 N. Nair, N. Wentzel and A. Jayaraman, *J. Chem. Phys.*, 2011, **134**, 194906.
19 T. B. Martin and A. Jayaraman, *Macromolecules*, 2013, **46**, 9144–9150.
20 N. Jouault, D. Lee, D. Zhao and S. K. Kumar, *Adv. Mater.*, 2014, **26**, 4031–4036.
21 S. E. Harton, S. K. Kumar, H. Yang, T. Koga, K. Hicks, H. Lee, J. Mijovic, M. Liu, R. S. Vallery and D. W. Gidley, *Macromolecules*, 2010, **43**, 3415–3421.
22 N. Jouault, D. Zhao and S. K. Kumar, *Macromolecules*, 2014, **47**, 5246–5255.
23 S. R. Raghavan, J. Hou, G. L. Baker and S. A. Khan, *Langmuir*, 2000, **16**, 1066–1077.
24 D. Zhao, M. D. Nicola, M. M. Khani, J. Jestin, B. C. Benicewicz and S. K. Kumar, *ACS Macro Lett.*, 2016, **5**, 790–795.
25 V. Pryamtisyn, V. Ganesan, A. Z. Panagiotopoulos, H. Liu and S. K. Kumar, *J. Chem. Phys.*, 2009, **131**, 221102.
26 B. Bozorgui, D. Meng, S. K. Kumar, C. Chakravarty and A. Cacciuto, *Nano Lett.*, 2013, **13**, 2732–2737.
27 A. H. Koch, G. Lévêque, S. Harms, K. Jaskiewicz, M. Bernhardt, A. Henkel, C. Sönnichsen, K. Landfester and G. Fytas, *Nano Lett.*, 2014, **14**, 4138–4144.
28 J. M. D. Lane and G. S. Grest, *Phys. Rev. Lett.*, 2010, **104**, 235501.
29 K. M. Salerno, A. E. Ismail, J. M. D. Lane and G. S. Grest, *J. Chem. Phys.*, 2014, **140**, 194904.
30 I. F. Hakem, A. M. Leech, J. D. Johnson, S. J. Donahue, J. P. Walker and M. R. Bockstaller, *J. Am. Chem. Soc.*, 2010, **132**, 16593–16598.
31 N. Jouault, P. Vallat, F. Dalmas, S. Said, J. Jestin and F. Boué, *Macromolecules*, 2009, **42**, 2031–2040.
32 J. F. Moll, P. Akcora, A. Rungta, S. Gong, R. H. Colby, B. C. Benicewicz and S. K. Kumar, *Macromolecules*, 2011, **44**, 7473–7477.
33 Q. Chen, S. Gong, J. Moll, D. Zhao, S. K. Kumar and R. H. Colby, *ACS Macro Lett.*, 2015, **4**, 398–402.